Morphology Development of Ultrathin Symmetric Diblock Copolymer Film via Solvent Vapor Treatment

Yu Xuan, Juan Peng, Liang Cui, Hanfu Wang, Binyao Li, and Yanchun Han*

State Key Laboratory of Polymer Physics and Chemistry, Changchun Institute of Applied Chemistry, Chinese Academy of Sciences, 5625 Renmin Street, Changchun 130022, P. R. China

Received February 2, 2004; Revised Manuscript Received July 5, 2004

ABSTRACT: We have followed the time development of the microdomain structure in symmetric diblock copolymer poly(styrene-*b*-methyl methacrylate), P(S-*b*-MMA), ultrathin films via PMMA-selective solvent vapor treatment by atomic force microscopy (AFM). After preparation on a substrate preferentially attracting the PMMA block, PS forms a continuous layer at a film's free surface. With subsequent solvent vapor treatment, the film gradually shows a well-ordered hexagonally packed nanocylinders structure. It is shown that only when the film thickness is less than the $^1/_2L_0$ (lamellar repeat spacing), and exposed to PMMA block selective solvent for an appropriate time, can the well-ordered hexagonally packed nanocylinders form. On an extended solvent vapor treatment, a mixed morphology containing nanocylinders and stripes appears, followed by the striped morphologies. When the annealing time is long enough, the film comes back to the flat surface again, however, with PMMA instead of PS dominating the free surface. Thickness confinement and solvent induced reconstruction of the film are shown to be responsible for the P(S-*b*-MMA) morphology and surface chemistry development.

Introduction

The ability of block copolymers (BCs) to form a rich variety of nanoscale periodic patterns[1−7] offers the potential to fabricate high-density arrays for use in data storage, electronics, molecular separation, combinatorial chemistry, and DNA screening, for example. For many applications where regular periodic arrays are required, it will be necessary to generate long-range alignment of nanostructures in block copolymer films.[1−42] This can be done in several ways: through the control of solvent evaporation,[30−38,56] controlled interfacial interactions,[1−7,57,58] using electric fields[15] or chemical or mechanical patterning,[1−7] by varying film thickness,[39−46] just name a few.

The preparation of BC thin films under various solvent evaporation conditions turns out to be a good way to manipulate the microstructures.[30−38] Krausch et al.[34] followed the time development of the microdomain structure in polystyrene-*block*-poly(2-vinylpyridine)-*block*-poly(*tert*-butyl methacrylate) triblock copolymer films during solvent vapor treatment. Upon swelling with THF vapor, lamellar developed originating from the free surface of the film and grew toward the substrate and eventually established a multiplayer structure throughout the film. Kim and Libera[31] demonstrated that, by controlling the solvent evaporation rate, both vertical and in-plane PS cylinders could be obtained in a PS/PB/PS triblock copolymer thin film for a thickness of ∼100 nm. It has recently been suggested that a necessary condition to produce perpendicular cylinders through solvent evaporation is that a good solvent for both blocks should be used and that one block only is below its glass transition temperature at room temperature. Another fast solvent extraction process resulted in a perpendicular lamellar microstructure.[30] The mechanical strain field present during the solvent drying process was discussed as the driving force for the observed microdomain structures.

* Corresponding author: e-mail ychan@ciac.jl.cn; Fax +86-431-5262126.

Besides the solvent evaporation, thickness is another important parameter in controlling order in BCs.[39−46] In thin films, the lamellae formed by symmetric block copolymers can orient either parallel or perpendicular to the substrate. Generally, the block with the lower surface energy tends to accumulate at the surface, resulting in an orientation of the phase-separated domains parallel to the interface, and a mismatch between the film thickness and lamellar period results in the holes or islands of height L_0 on the free surface of thin films. More complicated behavior is exhibited by BCP thin systems for film thickness less than L_0, for example, symmetric hybrid structure, antisymmetric hybrid structure,[1,35,40] etc.

In this paper, we have followed the time development of the microdomain structure in symmetric diblock copolymer poly(styrene-*b*-methyl methacrylate) P(S-*b*-MMA) ultrathin films (less than L_0) via PMMA-selective solvent vapor treatment by AFM. By well controlling the film thickness (less than $^1/_2L_0$), the selectivity of the solvent, and exposure time to PMMA block selective solvent, a hexagonally ordered nanocylinders in symmetric diblock copolymer P(S-*b*-MMA) thin film can form. Meanwhile, the surface chemistry can be changed. After preparation on a substrate preferentially attracting the PMMA block, PS forms a continuous layer at a film's free surface. On an extended solvent vapor treatment, the film gradually undergoes several metastable structures and finally comes back to the flat surface again, however, with PMMA instead of PS dominating the free surface. Thickness confinement and solvent-induced reconstruction of the film are shown to be responsible for the P(S-*b*-MMA) morphology and surface chemistry development.

Experimental Section

Sample Preparation. The symmetric diblock copolymers of P(S-*b*-MMA) (M_{PS} = 133 000, M_{PMMA} = 130 000, polydispersity M_w/M_n = 1.10, lamellae spacing L_0 of 90 nm) were purchased from Polymer Source Inc. The copolymer was dissolved in purified tetrahydrofuran (THF) to form solutions with four different concentrations (0.4, 0.6, 0.8, and 1.0 wt %).

10.1021/ma0497761 CCC: $27.50
Published on Web 08/25/2004

The solutions were spin-coated onto the freshly cleaned silicon wafers with native oxide cover to produce thin films with four different film thickness. All the prepared films were dried at 50 °C in a vacuum for 24 h to remove residual solvent. The film thickness was measured by ellipsometer (AUEL-III, Xi'an, China).

Sample Treatment. Three different methods were used to treat the samples. In the first group, the as-cast films with four different film thickness were exposed to the saturated chloroform vapor in a closed vessel and kept at room temperature for 60 h. In the second group, the as-cast film with thickness of 38 nm was chosen and exposed to four different solvent vapors (chloroform, acetone, toluene, carbon disulfide) in a closed vessel and kept at room temperature for 60 h. In the third group, the as-cast film with thickness of 38 nm was exposed to chloroform vapor for different periods. After certain duration of the treatment, the sample was removed to ambient atmosphere and promptly dried.

To exam the morphology of the bottom of the film, one film exposed to chloroform vapor for 60 h was floated onto a water bath and then transferred to the Si substrate with the bottom of the film up.

Atomic Force Microscopy (AFM) Characterization and X-ray Photoelectron Spectroscopy (XPS) Characterization. Atomic force microscopy (AFM) measurements were performed on SPA300HV with an SPI3800 controller, Seiko Instruments Industry, Co., Ltd. The images were taken with the tapping mode, and phase images were performed simultaneously with topographical imaging. The XPS was measured with VG ESCALAB MK at room temperature by using an Mg Kα X-ray source ($h\nu = 1253.6$ eV) at 14 kV and 20 mA. The sample analysis chamber of the XPS instrument was maintained at a pressure of 1×10^{-7} Pa.

Results and Discussion

Solvent Vapor Treatment Time Effect. After exposed to saturated chloroform vapor in a closed chamber at room temperature for different periods, the samples of symmetric P(S-*b*-MMA) thin film (38 nm) are removed to ambient atmosphere and promptly dried. The effect of solvent vapor treatment time on the P(S-*b*-MMA) thin film morphology is described by Figure 1. As annealed in saturated chloroform vapor for 10 h, the films appear laterally homogeneous in the optical micrographs. Accordingly, the film surface appears flat and featureless in the AFM topographic and phase images (Figure 1a,b). With the annealing time increase to 20 and 40 h, the film shows a highly disordered microstructure with evidence of microphase separation but no long-range order (Figure 1c−f). Prolonged exposure to saturated chloroform vapor (60 h) eventually leads to a well-ordered hexagonally packed nanocylinders structure with diameter of 43 nm and center-to-center interval of 90 nm (Figure 1g,h). After an extended duration of the treatment further (80 h), a mixed morphology containing nanocylinders and stripes appears with a little broadened diameter of 45 nm and little changed interval size (Figure 1i,j). With the treatment time increasing to 100 h, nanocylinders completely develop into stripes with the repeat spacing of 90 nm (Figure 1k,l). When the annealing time long enough (120 h), the film comes back to the flat surface again (Figure 1m,n).

It is known that an important issue for any nanostructure application of films is the axial extension of the nanostructures; i.e., it is essential that individual microdomains traverse the entire film thickness rather than forming unconnected domains across the film. In our case, this issue is addressed in Figure 2, which shows the AFM topographic (Figure 2a) and its corresponding phase contrast (Figure 2b) images of the backside of the ordered depression structure (Figure 1g,h), confirming that the PMMA domains span the entire film thickness. The diameter of the cylinders is a little larger than that seen in Figure 1g, indicating that the PMMA content near the substrate is more than that near the free surface. The favorable interaction between PMMA and the Si substrate is the major factor in the formation of larger pores at the bottom. Both the top (Figure 1g) and bottom (Figure 2a) of the film show holelike morphology. Since the chloroform content in the PMMA-rich microdomains is higher than that in PS domains, when the lower solubility PS phase solidifies, the higher solubility PMMA phase still contains some solvent. It will therefore continue to shrink on solvent extraction, resulting in a lower position compared with PS domains.

A previous description[47−50] has shown that when symmetric P(S-*b*-MMA) is cast on a Si substrate with a SiO_x surface layer, the PMMA preferentially segregates to the substrate while the PS segregates to the air interface due to the presence of asymmetric boundary condition. Therefore, in our case, it is reasonable to consider that after spin-coated onto the wafer substrate, PMMA dominates on the substrate interface and PS forms a continuous layer at a film's free surface. Since the PMMA block is more soluble in the chloroform solvent, there is a strong attractive interaction between the polymer and the solvent, and the net interaction between the polymer segments is repulsive. As a result, the coiled chains start to swell as soon as they are in contact with the solvent molecules. Diffusion of solvent to the surface can play a controlling role in defining the morphology. In P(S-*b*-MMA), the various microphase-separated morphologies observed are a clear function of the solvent treatment time. Elevated solvent treatment time increases the diffusivity of the polymer component in the thin film. Given enough time under conditions of relatively high diffusivity, the films will adopt their thermodynamically stable state. Less time effectively freezes in some metastable microstructure. With the increasing vapor treatment time, more and more PMMA occupies the film surface. The confirmation of the migration of the PMMA block to the surface is obtained by XPS with the tilting angle of 5°. Figure 3a−c shows that carbonyl peak at 288.5 eV binding energy has increased gradually from zero, and the $\pi-\pi$ peak for the phenyl ring around 292 eV has decreased gradually with increasing the PMMA selective solvent treatment time. This suggests the moving of PMMA to the top surface. Furthermore, water contact angle (CA) measurement results show that the CA changes from 92° of the surface of Figure 1a to 68° of the surface of Figure 1m. Since the water contact angle of PS homopolymer film is 90° and that of PMMA film is 66°, the changing of CA further suggests the migration of PMMA to the top surface. Therefore, after treatment in saturated chloroform vapor in a closed chamber at room temperature for certain period, the surface chemistry changes from PS to PMMA. The film (Figure 1g,h) with ordered morphology is also checked by XPS with varying tilting angle, 5°, 45 °, and 90° (Figure 4). The increasing of the tilting angle means the increasing of the checked depth from film surface. We can see that, with the increasing of the tilting angle, the carbonyl peak (Figure 4A) and oxygen peak area (Figure 4B) increase and the phenyl ring peak decreases (Figure 4A), indicating that

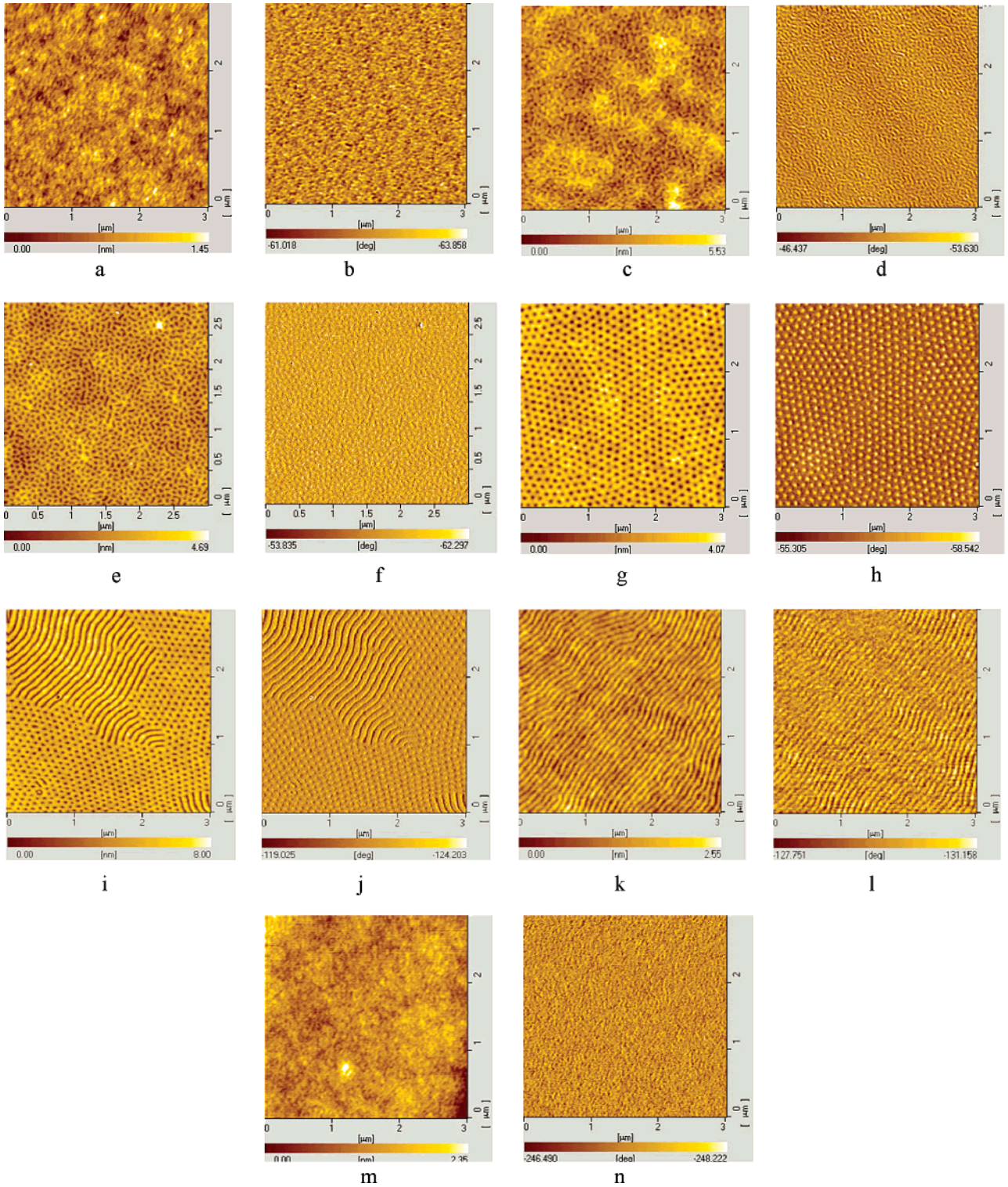

Figure 1. AFM topographic and phase images of symmetric P(S-*b*-MMA) thin films exposed to chloroform vapor for different times: (a, b) 10 h; (c, d) 20 h; (e, f) 40 h; (g, h) 60 h; (i, j) 80 h; (k, l) 100 h; (m, n) 120 h. (b), (d), (f), (h), (j), (l), and (n) are the corresponding phase contrast images of (a), (c), (e), (g), (i), (k), and (m), respectively.

the content of PMMA increases and PS decreases from surface down. The backside of the film (Figure 1m) is also checked by XPS with the tilting angle of 5° (Figure 5). The carbonyl peak and phenyl ring are still apparent. That shows that the bottom is covered by PMMA and PS. PMMA is pinned on the substrate due to its interaction with the SiO_x and follows the stretched conformation to surface due to its selective solvent strong attraction. PS takes the collapse conformation bending to the substrate.

Film Thickness Effect. From the above discussion, it is shown that well-ordered hexagonally packed nanocylinders in symmetric P(S-*b*-MMA) thin films can form. One may ask, what is the thickness effect on its formation? Figure 6 shows the film thickness effect on the symmetric P(S-*b*-MMA) thin films exposed to chloroform vapor for 60 h. Film thickness of symmetric P(S-*b*-MMA) is controlled by the solution concentration. Concentrations of 0.4, 0.6, 0.8, and 1 wt % are corresponding to the film thickness of 19, 26, 38, and 54 nm,

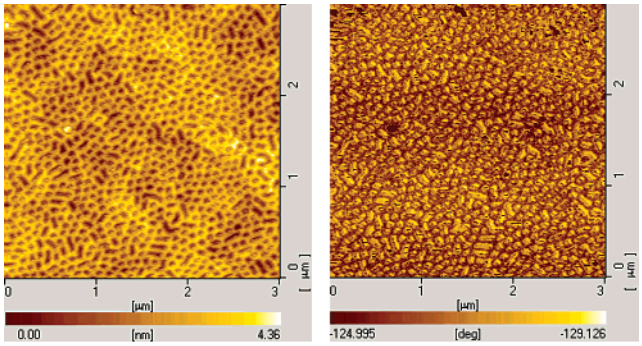

Figure 2. AFM topographic (a) and phase (b) images of the backside of the film of Figure 1g.

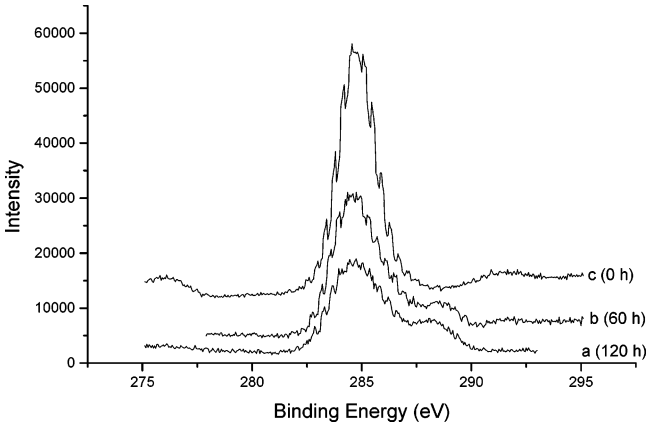

Figure 3. XPS (with the tilting angle of 5°) spectra in the C1 region: (a) the film treated in chloroform vapor for 120 h, (b) the film treated in chloroform vapor for 60 h, and (c) the as-cast copolymer film. For clarity, trace b is offset by 2000 in intensity and trace c is offset by 8000 in intensity.

respectively. Well-ordered hexagonally packed cylinders with diameter of 43 nm and center-to-center interval of 90 nm were obtained when the film thickness reaches 19, 26, and 38 nm, less than $^1/_2L_0$. While, when the film thickness is greater than $^1/_2L_0$, i.e., 54 nm, surface-perpendicular lamellar microphase morphology, which is the typical equilibrium state phase structure in the thin symmetric diblock copolymer films, can be obtained (Figure 6g,h). Figure 6h is the corresponding phase contrast image of Figure 6g. It is because when the film thickness is greater than $^1/_2L_0$, there are surplus copolymers above a single PS and PMMA layer. That weakens the absorbance of solvent to PMMA and hinders the movement of PMMA upward. Parts b, d, and f of Figure 6 are the corresponding phase contrast images of parts a, c, and e, respectively. At room temperature, the PMMA is harder than PS block. Thus, the PMMA phase is brighter and the PS phase is darker in phase contrast images. Therefore, the resulting surface morphology is well-ordered hexagonally packed PMMA blocks surrounded by PS blocks.

Solvent Selectivity Effect. The miscibility between a polymer and a solvent is governed by the polymer−solvent interaction parameter χ_{PS} (S = solvent and P = polymer). Using the Flory−Huggins criterion, the complete solvent−polymer miscibility can be realized when $\chi_{PS} < 0.5$. The smaller the value is, the stronger the affinity between solvent and polymer is. According to the literature[51−53] and the expression $\chi_{PS} = V_s[(\delta_{dS} - \delta_{dP})^2 + (\delta_{pS} - \delta_{pP})^2]/RT$, where V_s is the molar volume of the solvent, R is the gas constant, δ_d is the dispersion

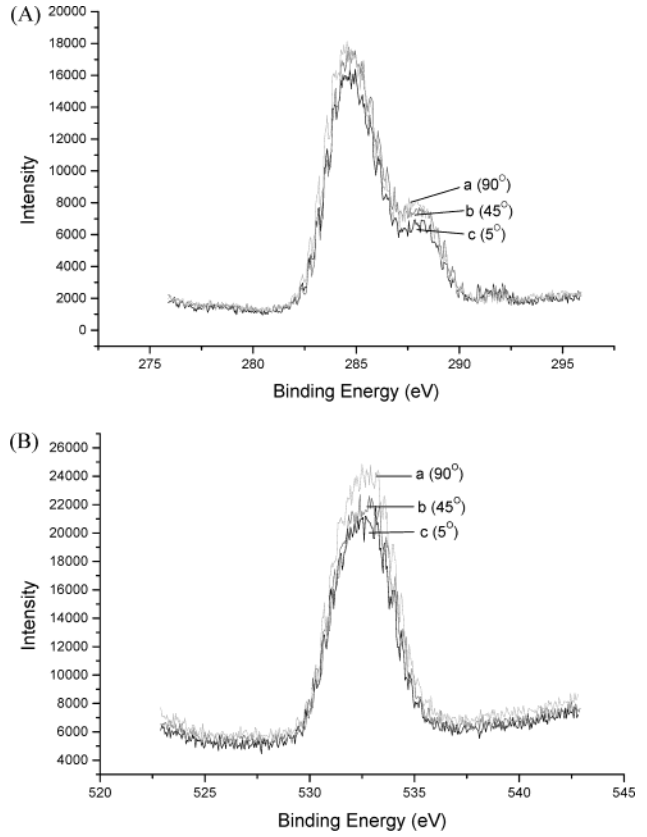

Figure 4. XPS spectra in the C1 (A) and O1 (B) regions of the sample of Figure 1g at different tilting angles: (a) 90°; (b) 45°; (c) 5°.

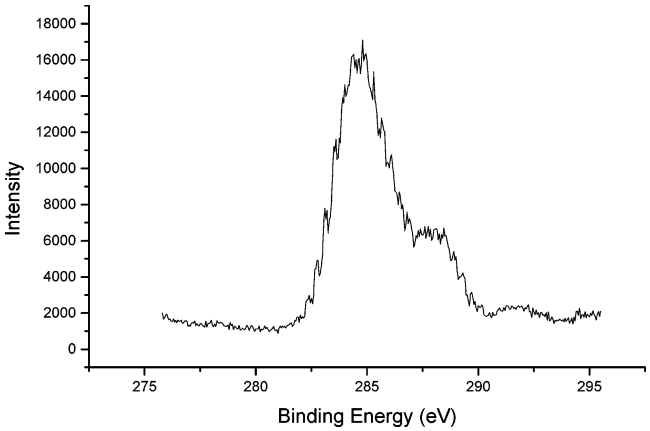

Figure 5. XPS (with the tilting angle of 5°) spectrum in the C1 region of the backside of Figure 1m.

solubility parameter, and δ_p is the polar solubility parameter, $\chi_{Chl-PMMAS} = 0.39$, $\chi_{Chl-PS} = 0.45$; $\chi_{Ace-PMMA} = 0.18$, $\chi_{Ace-PS} = 1.1$; $\chi_{Tol-PMMA} = 0.45$, $\chi_{Tol-PS} = 0.34$; and $\chi_{CS2-PMMA} = 1.2$, $\chi_{CS2-PS} = 0.01$. Thus, chloroform and acetone are both selective solvents for PMMA. Chloroform is slightly selective and acetone is strongly selective. Toluene and carbon disulfide are both selective solvents for PS. Toluene is slightly selective, and carbon disulfide is strongly selective.

The formation of well-ordered hexagonally packed cylinders is relative not only to the film thickness but also to the selectivity of the solvent vapor. To investigate the effect of the selectivity of the solvent on the microphase morphology, the films are exposed to four different solvent vapors (chloroform, acetone,[54] toluene, carbon disulfide). Figure 7a−h shows the AFM topog-

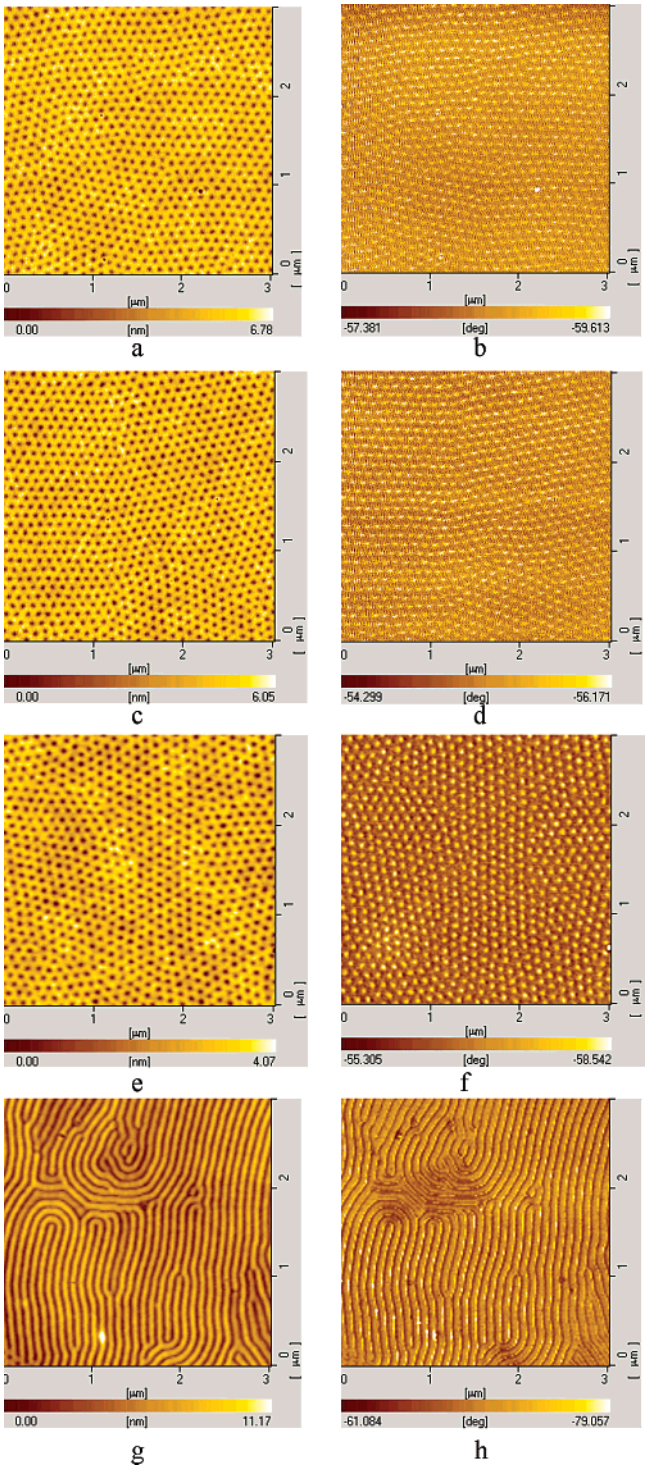

Figure 6. AFM topographic and phase images of symmetric P(S-*b*-MMA) thin film with different film thicknesses exposed to chloroform vapor for 60 h: (a, b) 19 nm; (c, d) 26 nm; (e, f) 38 nm; (g, h) 54 nm. (b), (d), (f), and (h) are the corresponding phase contrast images of (a), (c), (e), and (g), respectively.

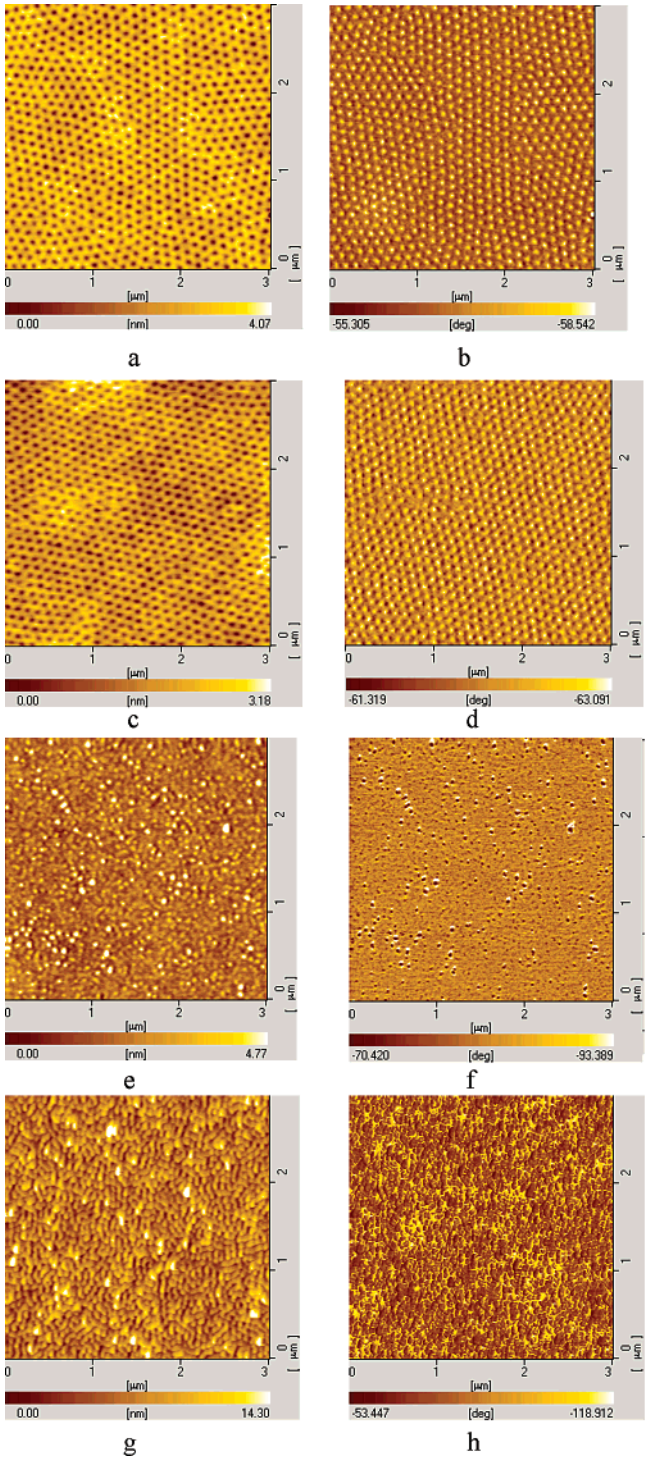

Figure 7. AFM topographic and phase images of thin symmetric P(S-*b*-MMA) film exposed to four different solvent vapors for 60 h: (a, b) chloroform; (c, d) acetone; (e, f) toluene; (g, h) carbon bisulfide. (b), (d), (f), and (h) are the corresponding phase contrast images of (a), (c), (e), and (g), respectively. The lighter regions are PMMA microdomains.

raphy and phase images of these films after exposed to the four solvent vapors for 60 h. From these images, we observe that only the films exposed to chloroform or acetone vapor exhibit ordered microphase morphology with diameter of 43 nm ($\approx {}^1/_2 L_0$) and center-to-center interval of 90 nm and that the films exposed to toluene or carbon disulfide vapor exhibit a macroscopically flat surface except for small protrusions. This fact illuminates that the ordered microphase morphology can be obtained only by exposing films to selective solvent vapor good for PMMA. Studies of block copolymer surfaces have shown that the lower surface energy constituent preferentially locates itself at the free surface. Green et al.[47,48] used XPS and Russell et al.[49,50] used SIMS and neutron scattering on diblock P(S-*b*-MMA) to show that, in the strong-segregation limit, the lower surface energy PS forms a continuous layer at a film's free surface. Therefore, when treated in PS-selective solvents, the upper boundary condition still

favors the PS, and the PS will continue to dominate the upper surface. However, the situation is different when treated in PMMA-selective solvent vapor. After placing the sample with PMMA preferentially segregates to the substrate into the saturated chloroform or acetone, the solvent imparts substantial mobility to the polymer. In addition, the solvent also mediates the interactions between the segments of the copolymer and reduces the differences in the surface energies of the components. Therefore, it causes the surface morphology development.

Zhao[55] used tethered P(S-*b*-MMA) to realize the changes in surface composition that are induced by different selective solvent treatment. In our study, if exposing a film which has inverted in response to a good PMMA solvent to a second solvent preferential to PS, i.e., CS_2, a reverted nanoprotrusion morphology is also observed.[54]

Discussion

It has been known that for a symmetric P(S-*b*-MMA) system, if the initial film thickness t is thicker than its equilibrium period L_0 and $t \neq (n + {}^1/_2)L_0$ (n an integer), islands or holes of height L_0 form at the free surface. However, when the film thickness is below L_0, its morphology is frustrated by the competition of several forces, including strong surface interactions, slow kinetics, and the "bulk" driving force toward a morphology with the natural period L_0.[43−46] A previous description has shown that when symmetric P(S-*b*-MMA) is cast on a Si substrate with a SiO_x surface layer, the PMMA preferentially segregates to the substrate while the PS segregates to the air interface due to the presence of asymmetric boundary condition. On exposure to chloroform or acetone vapor (selective solvents for PMMA), initially the chloroform or acetone vapor penetrates the PMMA microdomains which results in an increased mobility of PMMA. Therefore, PMMA is highly mobile and can reconstruct itself easily. With the continuous increasing of the annealing time, more and more PMMA enriched at the SiO_x substrate migrate to the surface due to the attraction by the chloroform or acetone vapor. Therefore, surface-perpendicular PMMA protrusions approximately $L_0/2$ in width perforate the PS layer in response to the chloroform or acetone attraction. With the film thickness less than ${}^1/_2L_0$, ordered hexagonally packed nanocylinders morphology exhibits to minimize the total energy. When the film thickness is larger than ${}^1/_2L_0$, the film has thicker PS layer at the film surface; elongated striped domains that are called perpendicular lamella (PL) with alternating light and dark regions perpendicular to the substrate form. Hence, with regard to the thickness of films, we realize that in this copolymer system there is a threshold film thickness T^* (${}^1/_2L_0$, here is 45 nm), above which the films exhibit surface-parallel or surface-perpendicular morphology as mentioned in previous studies and below which the films undergo unconventional morphology of well-ordered hexagonally packed cylinders by selective solvent vapor treatment.

We bring forward a mechanism of solvent vapor annealing for this case. As cast, since PMMA has a favorable interaction with the native silicon oxide, the surface tension of PS is comparatively lower ($\gamma_{PS} = 40.7$ mJ/m^2, $\gamma_{PMMA} = 41.1$ mJ/m^2);[33,59] thus, this system favors asymmetric morphologies that have PS-rich layer at the free surface and PMMA-rich layer at the substrate (Figure 8a). When exposed to selective solvent vapor good for PMMA, the films is covered with solvent molecules. In this vapor environment, the boundary condition is different from that in the air or in a vacuum. Both Si substrate and solvent vapor layer at film surface absorb PMMA preferentially; for PMMA−solvent the interaction parameter is less than the PS−solvent interaction parameter ($\chi_{PMMA-S} < \chi_{PS-S}$). Solvent vapor molecules have a stronger tendency to attract PMMA than PS to maximize the PMMA−solvent contacts, so PMMA is pulled toward the film surface (Figure 8b). With the increasing of vapor treatment time, more and more PMMA occupied the film surface. The confirmation of the migration of the PMMA block to the up surface is obtained by XPS (Figures 3 and 4) and water contact angle meansurement. When treated in chloroform vapor for certain time (i.e., 60 h), the polymer chains are frozen by moving out from the solvent vapor environment and dried quickly. Ordered hexagonally packed structure is obtained to minimize the system total energy in case of PMMA uprising (Figure 8c,d). After an extended duration of the treatment further, surface-perpendicular morphology appears (Figure 8e,f). For a long enough treatment time (120 h), due to the interaction of PMMA between the Si substrate and the solvent, the PMMA block takes the stretched conformation and the PS block takes the collapse conformation. Therefore, PMMA occupies the upper surface and the partial substrate regions (Figure 8g,h).

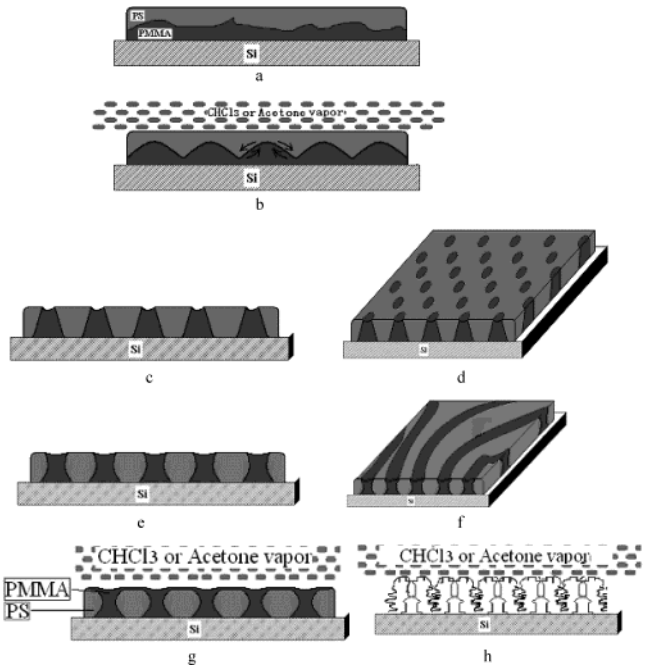

Figure 8. Schematic model of time development of the microstrcuture formation of thin symmetric P(S-*b*-MMA) film. The black regions denote PMMA, the gray regions denote PS, and the dots denote solvent vapor molecules. (a) Before being exposed to chloroform or acetone vapor, PS dominates the free surface. (b) Exposed to chloroform or acetone vapor for a certain time, PMMA begins to go to the surface. (c) Cross-section view of nanocylinder formation. (d) Plane view of (c). (e) Cross-section view of the lamellar formation. (f) Plane view of (e). (g) After a long time annealing, PMMA dominates the free surface. PMMA block takes the stretched conformation, and PS block takes the collapse conformation (h).

Why is the microphase morphology of the films exposed to chloroform or acetone vapor a hexagonally packed nanodepression rather than nanodots? This is because chloroform or acetone is a selectively good

solvent for the PMMA block of the diblock copolymer. This causes different swelling degree of PMMA and PS in the solvent vapor environment. The solvent content in the PMMA-rich microdomains is higher than that in the PS-rich microdomains. Hence, after drying, the shrinkage of the PMMA block is higher than that of the PS block in the film, leaving nanoholes on the surface.

Conclusions

We have followed the time development of the microdomain structure in the symmetric diblock copolymer poly(styrene-*b*-methyl methacrylate), P(S-*b*-MMA), ultrathin films via PMMA-selective solvent vapor treatment by AFM. By well controlling the film thickness (less than $^1/_2L_0$), the selectivity of the solvent, and exposure time to PMMA block selective solvent, the well-ordered hexagonally packed nanocylinders can form. Furthermore, the surface chemistry can be changed. After preparation on a substrate preferentially attracting the PMMA block, PS forms a continuous layer at a film's free surface. On an extended solvent vapor treatment, the film gradually undergoes several metastable structures and finally comes back to the flat surface again, however, with PMMA instead of PS dominating the free surface. Thickness confinement and solvent-induced reconstruction of the film are shown to be responsible for the P(S-*b*-MMA) morphology and surface chemistry development.

Acknowledgment. This work is subsidized by the National Natural Science Foundation of China (50125311, 20334010, 20274050, 50390090, 50373041), the Ministry of Science and Technology of China (2003CB615601, 2002CCAD4000), and the Chinese Academy of Sciences (Distinguished Talents Program, KJCX2-SW-H07).

References and Notes

(1) Fasolka, M. J.; Mayes, A. M. *Annu. Rev. Mater. Res.* **2001**, *31*, 323.
(2) Hamley, I. W. *Nanotechnology* **2003**, *14*, R39−R54.
(3) Park, C.; Yoon, J.; Thomas, E. L. *Polymer* **2003**, *44*, 6725.
(4) Hamley, I. W. *The Physics of Block Copolymers;* Oxford University Press: New York, 1998.
(5) Förster, S.; Antonietti, M. *Adv. Mater.* **1998**, *10*, 195.
(6) Förster, S.; Plantenberg, T. *Angew. Chem., Int. Ed.* **2002**, *41*, 688.
(7) Hamley, I. W. *Angew. Chem., Int. Ed.* **2003**, *42*, 1692.
(8) Konodo, Y.; Takayanah, K. *Science* **2000**, *289*, 606.
(9) Fritzsche, W.; Böhm, K. J.; Unger, E.; Köhler, J. M. *Appl. Phys. Lett.* **1999**, *75*, 2845.
(10) Alivesatos, A. P. *Science* **1996**, *271*, 933.
(11) Ashoori, R. C. *Nature (London)* **1996**, *379*, 413.
(12) Morales, A. M.; Lieber, C. M. *Science* **1998**, *279*, 208.
(13) Black, C. T.; Guarini, K. W.; Milkove, K. R.; Baker, S. M.; Russell, T. P.; Tuominen, M. T. *Appl. Phys. Lett.* **2001**, *79*, 409.
(14) Huang, E.; Rockford, L.; Russell, T. P.; Hawker, C. J.; Mays, J. *Nature (London)* **1998**, *395*, 757.
(15) Morkved, T. L.; Lu, M.; Urbas, A. M.; Ehrichs, E. E.; Jaeger, H. M.; Russell, T. P. *Science* **1996**, *273*, 931.
(16) Chen, Z. R.; Kornfield, J. A.; Smith, S. D.; Grothaus, J. T.; Satkowski, M. M. *Science* **1997**, *277*, 1248.
(17) Sivaniah, E.; Hayashi, Y.; Iino, M.; Hashimoto, T.; Fukunaga, K. *Macromolecules* **2003**, *36*, 5894.
(18) Peters, R. D.; Yang, X. M.; Wang, Q.; Pablo, J. J.; Nealy, P. F. *J. Vac. Sci. Technol. B* **2000**, *18*, 3530.
(19) Segalman, R. A.; Yokohama, H.; Kramer, E. J. APS Meeting, Minneapolis, MN, March 20−24, 2000.
(20) Mansky, P.; DeRouchey, J.; Russell, T. P.; Mays, J.; Pitsikalis, M.; Morkved, T.; Jaeger, H. *Macromolecules* **1998**, *31*, 4399.
(21) Huang, E.; Russell, T. P.; Harrison, C.; Chaikin, P. M.; Register, R. A.; Hawker, C. J.; Mays, J. *Macromolecules* **1998**, *31*, 7641.
(22) Mansky, P.; Russell, T. P.; Hawker, C. J.; Pitsikalis, M.; Mays, J. *Macromolecules* **1997**, *30*, 6810.
(23) Yang, X. M.; Peters, R. D.; Nealey, P. F.; Solak, H. H.; Cerrina, F. *Macromolecules* **2000**, *33*, 9575.
(24) Peters, R. D.; Yang, X. M.; Nealey, P. F. *Macromolecules* **2002**, *35*, 1822.
(25) Thurn-Albrecht, T.; Schotter, J.; Kastle, A.; Emley, N.; Shibauchi, T.; Krusin-Elbaum, L.; Guarini, K.; Black, C. T.; Tuominen, M. T.; Russell, T. P. *Science* **2000**, *290*, 2126.
(26) Thurn-Albrecht, T.; Derouchey, J.; Russell, T. P.; Jaeger, H. M. *Macromolecules* **2000**, *33*, 3250.
(27) Jeong, U.; Kim, H. C.; Rodriguez, R. L.; Tsai, I. Y.; Stafford, C. M.; Kim, J. K.; Hawker, C. J.; Russell, T. P. *Adv. Mater.* **2002**, *14*, 274.
(28) Xu, T.; Stevens, J.; Villa, J. A.; Goldbach, J. T.; Guarini, L. W.; Black, C. T.; Hawker, C. J.; Russell, T. P. *Adv. Funct. Mater.* **2003**, *13*, 698.
(29) Jeong, U.; Ryu, D. Y.; Kim, J. K.; Kim, D. H.; Russell, T. P.; Hawker, C. J. *Adv. Mater.* **2003**, *15*, 1247.
(30) Fukunaga, K.; Elbs, H.; Magerle, R.; Krausch, G. *Macromolecules* **2000**, *33*, 947.
(31) Kim, G.; Libera, M. *Macromolecules* **1998**, *31*, 2569.
(32) Hanley, K. J.; Lodge, T. P.; Huang, C. I. *Macromolecules* **2000**, *33*, 5918.
(33) Niu, S.; Saraf, R. F. *Macromolecules* **2003**, *36*, 2428.
(34) Fukunaga, K.; Hashimoto, T.; Elbs, H.; Krausch, G. *Macromolecules* **2002**, *35*, 4406.
(35) Fasolka, M. J.; Banerjee, P.; Mayes, A. M. *Macromolecules* **2000**, *33*, 5702.
(36) Buck, E.; Fuhrmann, J. *Macromolecules* **2001**, *34*, 2172.
(37) Temple, K.; Kulbaba, K.; Power-Billard, K. N.; Manners, I.; Leach, K. A.; Xu, T.; Russell, P. T.; Hawker, C. J. *Adv. Mater.* **2003**, *15*, 297.
(38) Lin, Z.; Kim, D. H.; Wu, X.; Boosahda, L.; Stone, D.; LaRose, L.; Russell, T. P. *Adv. Mater.* **2002**, *14*, 1373.
(39) Tang, W. H.; Witten, T. A. *Macromolecules* **1998**, *31*, 3130.
(40) Morkved, T. L.; Jaeger, J. M. *Europhys. Lett.* **1997**, *40*, 643.
(41) Elbs, H.; Drummer, C.; Abetz, V.; Krausch, G. *Macromolecules* **2002**, *35*, 5570.
(42) Russell, T. P.; Menelle, A.; Anastasiadis, S. H.; Satija, S. K.; Majkrzak, C. F. *Macromolecules* **1991**, *24*, 6263.
(43) Fasolka, M. J.; Harris, D. J.; Mayes, A. M. *Phys. Rev. Lett.* **1997**, *79*, 3018.
(44) Turner, M. S.; Joanny, J. F. *Macromolecules* **1992**, *25*, 6681.
(45) Walton, D. G.; Kellogg, G. J.; Mayes, A. M.; Lambooy, P.; Russell, T. P. *Macromolecules* **1994**, *27*, 6225.
(46) Radzilowski, L. H.; Carvahlo, B. L.; Thomas, E. L. *J. Polym. Sci.* **1996**, *34*, 3081.
(47) Green, P. F.; Christenson, T. M.; Russell, T. P.; Jerome, R. *J. Chem. Phys.* **1990**, *92*, 1478.
(48) Green, P. F.; Christenson, T. F.; Russell, T. P. *Macromolecules* **1991**, *24*, 252.
(49) Anastasiadis, S. H.; Russell, T. P.; Satija, S. K.; Majkrzak, C. F. *Phys. Rev. Lett.* **1989**, *62*, 1852.
(50) Russell, T. P.; Coulon, G.; Deline, V. R.; Miller, D. C. *Macromolecules* **1989**, *22*, 4600.
(51) Chen, S. A. *J. Appl. Polym. Sci.* **1971**, *15*, 1247.
(52) Van Krevelen, D. W. *Properties of Polymers;* Elsevier Scientific Publishing Co.: Amsterdam, 1976.
(53) Brandrup, J.; Immergut, E. H.; Grulke, E. A. *Polymer Handbook*, 4th ed.; John Wiley & Sons: New York, 1999.
(54) Peng, J.; Xuan, Y.; Han, Y. C. *J. Chem. Phys.* **2004**, *120*, 11163.
(55) Zhao, B.; Brittain, W. J. *J. Am. Chem. Soc.* **1999**, *121*, 3557.
(56) Kim, S. H.; Misner, M. J.; Xu, T.; Kimura, M.; Russell, T. P. *Adv. Mater.* **2004**, *16*, 226.
(57) Xu, T.; Stevens, J.; Villa, J. A.; Goldbach, J. T.; Guarini, K. W.; Black, C. T.; Hawker, C. J.; Russell, T. P. *Adv. Funct. Mater.* **2003**, *13*, 698.
(58) Xu, T.; Goldbach, J. T.; Misner, M. J.; Kim, S.; Gibaud, A.; Gang, O.; Ocko, B.; Guarini, K. W.; Black, C. T.; Hawker, C. J.; Russell, T. P. *Macromolecules* **2004**, *37*, 2972.
(59) Costa, A. C.; Geoghegan, M.; Vlcek, P.; Composto, R. J. *Macromolecules* **2003**, *36*, 9897.

MA0497761